

caused by slow oxidation of the electrolyte by the fully charged manganese oxide, corrosion at the current collector interfaces, and/or mass transfer effects. These phenomena can easily be minimized by lowering the voltage limit upon charge, improving electrolyte compositions and current collector materials, and by judicious use of rest periods between half-cycles. At any rate, these early results demonstrate that the orthorhombic sodium manganese oxide is remarkably stable and undergoes alkali metal intercalation processes readily and reversibly.

### Conclusions

The suitability of the orthorhombic sodium manganese oxide for use as a cathode material in alkali metal secondary batteries has been demonstrated. This material, which has never before been used in a battery, has high specific capacity in both lithium and sodium cells, and discharge characteristics suitable for use with polymer electrolytes. An especially striking feature is the excellent reversibility and stability upon cycling in lithium cells.

### Acknowledgment

This work was supported by the Assistant Secretary for Energy Efficiency and Renewable Energy, Office of Transportation Technologies, Electric and Hybrid Propulsion Division of the U.S. Department of Energy under Contract No. DE-AC03-76SF00098. We would like to thank Dr. Thomas Richardson of Lawrence Berkeley Laboratory for many helpful discussions.

Manuscript received July 12, 1994; revised manuscript received July 26, 1994.

Lawrence Berkeley Laboratory assisted in meeting the publication costs of this article.

### REFERENCES

1. *Structural Inorganic Chemistry*, 4th ed., A. F. Wells, Editor, pp. 449-450, Clarendon Press, Oxford (1975).
2. K. M. Parida, S. B. Kanungo, and B. R. Sant, *Electrochim. Acta*, **26**, 435 (1981).
3. M. M. Thackeray, A. de Kock, M. H. Roussow, D. Liles, R. Bittihn, and D. Hoge, *This Journal*, **139**, 363 (1992).
4. D. Guyomard and J. M. Tarascon, *ibid.*, **140**, 3071 (1993).
5. Q. Xu and G. Wan, *J. Power Sources*, **41**, 315 (1993).
6. T. Ohzuku, M. Kitagawa, K. Sawai, and T. Hirai, *This Journal*, **138**, 360 (1991).
7. J.-P. Parant, R. Olazcuaga, M. DeValette, C. Fouassier, and P. Hagenmuller, *J. Solid State Chem.*, **3**, 1 (1971).
8. A. Mendiboure, C. Delmas, and P. Hagenmuller, *ibid.*, **57**, 323 (1985).
9. L. R. Pederson, G. D. Maupin, W. J. Weber, D. J. McReady, and R. W. Stephens, *Mat. Lett.*, **10**, 437 (1991).
10. Y. Ma, M. M. Doeff, S. J. Visco, and L. C. De Jonghe, *This Journal*, **140**, 2726 (1993).
11. (a) R. J. Gummow and M. M. Thackeray, *ibid.*, **141**, 1178 (1994); (b) R. J. Neat and R. J. Powell, U.S. Pat. 5,030,523 (1991).
12. R. Koksang, I. I. Olsen, P. E. Tonder, N. Knudsen, and D. Fauteux, *J. Appl. Electrochem.*, **21**, 301 (1991).

# Spinel Anodes for Lithium-Ion Batteries

E. Ferg, R. J. Gummow, and A. de Kock

CSIR, Division of Materials Science and Technology, Pretoria 0001, South Africa

M. M. Thackeray\*

Argonne National Laboratory, Electrochemical Technology Program, Chemical Technology Division, Argonne, Illinois 60439

### ABSTRACT

Anodes of  $\text{Li}_4\text{Mn}_5\text{O}_{12}$ ,  $\text{Li}_4\text{Ti}_5\text{O}_{12}$ , and  $\text{Li}_2\text{Mn}_4\text{O}_9$  with a spinel-type structure have been evaluated in room-temperature lithium cells. The cathodes that were selected for this study were the stabilized spinels,  $\text{Li}_{1.03}\text{Mn}_{1.97}\text{O}_4$  and  $\text{LiZn}_{0.025}\text{Mn}_{1.95}\text{O}_4$ , and layered  $\text{LiCoO}_2$ . The electrochemical data demonstrated that  $\text{Li}^+$  ions will shuttle between two transition-metal host structures (anode and cathode) at a reasonably high voltage with a concomitant change in the oxidation state of the transition metal cations so that the  $\text{Li}^+$  ions do not reduce to the metallic state at the anode during charge. These cells reduce the safety hazards associated with cells containing metallic-lithium, lithium-alloy, and lithium-carbon anodes.

The principle of using the  $[\text{B}_2]\text{X}_4$  framework of an  $\text{A}[\text{B}_2]\text{X}_4$  spinel as a stable host structure for anodes and cathodes of rechargeable lithium cells was demonstrated several years ago.<sup>1,2</sup> To achieve an acceptably high cell voltage, the spinel anode should provide a relatively low cell voltage against metallic lithium, whereas the cathode should provide a relatively high voltage against lithium. Over the past 10 years many lithium spinels (*i.e.*, those with lithium on the A-sites, and B = Ti, V, Mn, Co Ni) have been evaluated as cathode materials in lithium or lithium-carbon cells,<sup>3,14</sup> several of which have been shown to be stable to electrochemical cycling. The working voltage of the cell depends on the B-cation, as shown in Table I.

Therefore, low-voltage spinels can be coupled with high-voltage spinels to fabricate cells with an intermediate voltage. For example, from Table I, it can be seen that  $\text{Li}_{2+x}\text{Mn}_4\text{O}_9/\text{Li}_{1-x}\text{Mn}_2\text{O}_4$  and  $\text{Li}_{4+x}\text{Mn}_5\text{O}_{12}/\text{Li}_{1-x}\text{Mn}_2\text{O}_4$  cells should operate at approximately 1.2 V, which is similar to the voltage of a nickel-cadmium cell, and that a  $\text{Li}_{4+x}\text{Ti}_5\text{O}_{12}/\text{Li}_{1-x}\text{Mn}_2\text{O}_4$  cell should operate at approximately twice the voltage of a nickel-cadmium cell (2.5 V). The operating principle of these lithium-ion or "rocking-chair" cells is well known and can, of course, be extended to other host structures, as has been demonstrated in the past.<sup>15</sup> Transition metal oxides that have been evaluated as anode materials include  $\alpha\text{-Fe}_2\text{O}_3$ ,<sup>16</sup>  $\text{MoO}_2$ ,<sup>17</sup> and  $\text{WO}_2$ .<sup>17</sup> More recently, Ohzuku has reported electrochemical

data for a  $\text{Li}_4\text{Ti}_5\text{O}_{12}/\text{LiNiO}_2$  cell.<sup>18</sup> In this paper we report preliminary data on the electrochemical performance of  $\text{Li}_2\text{Mn}_4\text{O}_9$ ,  $\text{Li}_4\text{Mn}_5\text{O}_{12}$ , and  $\text{Li}_4\text{Ti}_5\text{O}_{12}$  spinel anodes against stabilized-spinel cathodes ( $\text{Li}_{1.03}\text{Mn}_{1.97}\text{O}_4$ ,  $\text{LiZn}_{0.025}\text{Mn}_{1.95}\text{O}_4$ ), and  $\text{LiCoO}_2$  in room-temperature cells.

### Experimental

The anode and cathode materials were synthesized by solid-state reactions using the precursor materials and reaction conditions summarized in Table II. Stoichiometric amounts of the reagents were used in all cases except for the  $\text{Li}_4\text{Ti}_5\text{O}_{12}$  anode, in

Table I. Electrochemical data of various Li-spinel cells.

Cell couple	$x_{\text{max}}$	Approximate operating voltage (V)
$\text{Li}/\text{Li}_{4+x}\text{Ti}_5\text{O}_{12}$	3	1.5
$\text{Li}/\text{Li}_{1+x}\text{V}_2\text{O}_4$	1	2.3 to 1.3 (two-stage)
$\text{Li}/\text{Li}_{2+x}\text{Mn}_4\text{O}_9$	3	2.8
$\text{Li}/\text{Li}_{4+x}\text{Mn}_5\text{O}_{12}$	3	2.8
$\text{Li}/\text{Li}_{2-x}\text{Co}_2\text{O}_4$	~1	3.4
$\text{Li}/\text{Li}_{1-x}\text{Mn}_2\text{O}_4$	~1	4.0

\* Electrochemical Society Active Member.

Table II. Reaction conditions for the preparation of anode and cathode materials.

	Precursor materials	Firing temperature (°C)	Firing time (h)
<b>Anode</b>			
Li <sub>2</sub> Mn <sub>4</sub> O <sub>9</sub>	LiOH · H <sub>2</sub> O, MnCO <sub>3</sub>	380	20
Li <sub>4</sub> Mn <sub>5</sub> O <sub>12</sub>	LiOH · H <sub>2</sub> O, MnCO <sub>3</sub>	380	20
Li <sub>4</sub> Ti <sub>5</sub> O <sub>12</sub>	Li <sub>2</sub> CO <sub>3</sub> , TiO <sub>2</sub>	1000	24
<b>Cathode</b>			
Li <sub>1.03</sub> Mn <sub>1.97</sub> O <sub>4</sub>	LiOH · H <sub>2</sub> O, γ-MnO <sub>2</sub>	650	48
LiZn <sub>0.025</sub> Mn <sub>1.95</sub> O <sub>4</sub>	LiOH · H <sub>2</sub> O, γ-MnO <sub>2</sub> , Zn(NO <sub>3</sub> ) <sub>2</sub> · 2H <sub>2</sub> O	650	48
LiCoO <sub>2</sub>	Li <sub>2</sub> CO <sub>3</sub> , CoCO <sub>3</sub>	900	24

which an 8% excess of Li<sub>2</sub>CO<sub>3</sub> was used to compensate for the loss of a small amount of Li<sub>2</sub>O during firing at 1000°C. Powder x-ray diffraction data obtained on an automated Rigaku diffractometer showed that the LiCoO<sub>2</sub> and spinel products were single phase and had patterns that were consistent with those reported in the literature.<sup>6,7,19-21</sup>

Electrochemical characteristics were determined from prismatic lithium cells with a flooded electrolyte configuration at room temperature (22°C). A full description of the cell design is given elsewhere.<sup>22</sup> A typical anode and cathode consisted of the transition metal oxide active material intimately mixed with either acetylene black and an ethylene-propylene-diene-monomer (EPDM) binder in a 90:7:3 ratio by mass, or with Teflon-acetylene black (TAB) in a 80:20 mass ratio. The TAB was mixed in a 1:2 mass ratio. The anode and cathode powders (20 to 30 mg) were compacted onto a stainless-steel mesh current collector, approximately 10 mm in diameter. A metallic lithium reference electrode, compacted onto a stainless-steel mesh, was used to monitor, independently, the voltages of the anode and cathode. The electrolyte consisted of a 1M solution of LiClO<sub>4</sub> in anhydrous propylene carbonate (Aldrich), which was used as received. The anode and cathode were separated by a microporous polypropylene separator (Celgard 3401). Cells were charged and discharged at a constant current of either 0.10 or 0.15 mA/cm<sup>2</sup>.

## Results and Discussion

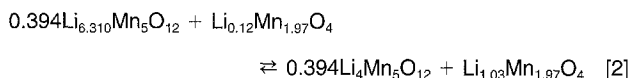
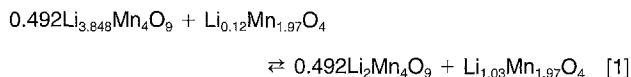
Table III gives the composition of the various anode and cathode materials that is reached at the maximum state of charge and discharge, as well as the theoretical capacity of each electrode based on the mass of the fully charged electrode. A major advantage of these lithium-ion cells is that they can be fabricated in the discharged state from stable materials that are fairly easy to prepare; these cells should, therefore, offer an excellent shelf life. Moreover, because the lithium ions are never reduced to the metallic state at the anode during charge, these cells will be much safer to use than those that employ metallic-lithium, lithium-alloy, or lithium-carbon anodes.

Cells were constructed such that they were cathode limited; they contained, in general, approximately 5 to 10% excess active anode material. The cathodes were selected on the basis that they were all high-voltage materials, *i.e.*, they deliver approximately 4 V vs. pure lithium. The spinel cathodes Li<sub>1.03</sub>Mn<sub>1.97</sub>O<sub>4</sub> and

LiZn<sub>0.025</sub>Mn<sub>1.95</sub>O<sub>4</sub> have recently been reported to be more stable to electrochemical cycling than the standard spinel LiMn<sub>2</sub>O<sub>4</sub>. The improved stability was attributed to the suppression of the Jahn-Teller effect; it was conjectured, particularly in deeply discharged cathodes, that the Jahn-Teller effect could occur on the surface of some of the particles at a relatively high voltage (>3.5 V), *i.e.*, before the overall cell voltage reached 3 V.<sup>7</sup> The Jahn-Teller effect in Li-Mn-O spinel cathodes occurs when the average Mn oxidation state reaches 3.5<sup>6</sup>; it reduces the crystal symmetry from cubic to tetragonal and significantly increases the *c/a* lattice-parameter ratio.<sup>6</sup> The anisotropic expansion/contraction of the unit cell that occurs during discharge/charge destroys the structural integrity of spinel cathodes and significantly reduces the cycling efficiency of the cells. In the stabilized spinels, Li<sub>1.03</sub>Mn<sub>1.97</sub>O<sub>4</sub> and LiZn<sub>0.025</sub>Mn<sub>1.95</sub>O<sub>4</sub>, the mean oxidation state of Mn is controlled to be marginally above 3.5 at the end of discharge to combat the onset of the Jahn-Teller distortion. In fully discharged Li<sub>1.03</sub>Mn<sub>1.97</sub>O<sub>4</sub> and Li<sub>1.025</sub>Zn<sub>0.025</sub>Mn<sub>1.95</sub>O<sub>4</sub> cathodes that have the stoichiometric spinel composition, the manganese-ion valency is 3.54 and 3.55, respectively.

The cells can be classified into those that provide an initial voltage of 1.2 V, and those that provide 2.5 V.

**1.2 V cells.**—The ideal reactions for full utilization of the anode and cathode materials in Li<sub>2</sub>Mn<sub>4</sub>O<sub>9</sub>/Li<sub>1.03</sub>Mn<sub>1.97</sub>O<sub>4</sub> and Li<sub>4</sub>Mn<sub>5</sub>O<sub>12</sub>/Li<sub>1.03</sub>Mn<sub>1.97</sub>O<sub>4</sub> cells are



In both reactions the valency of the manganese ions in the anode and cathode varies during charge and discharge between 3.54 and 4.00; in principle, the Jahn-Teller effect is therefore avoided at all states of charge and discharge. The theoretical cell capacities for reactions 1 and 2, based on the masses of the electrode materials only, are 67 and 65 Ah/kg, respectively; the theoretical energy density of each cell, based on a constant discharge voltage of 1.2 V is, therefore, 80 and 78 Wh/kg. By analogy, a nickel-cadmium cell that discharges according to the ideal reaction



has a theoretical capacity of 162 Ah/kg; at a constant 1.2 V discharge it has a theoretical energy density of 194 Wh/kg.

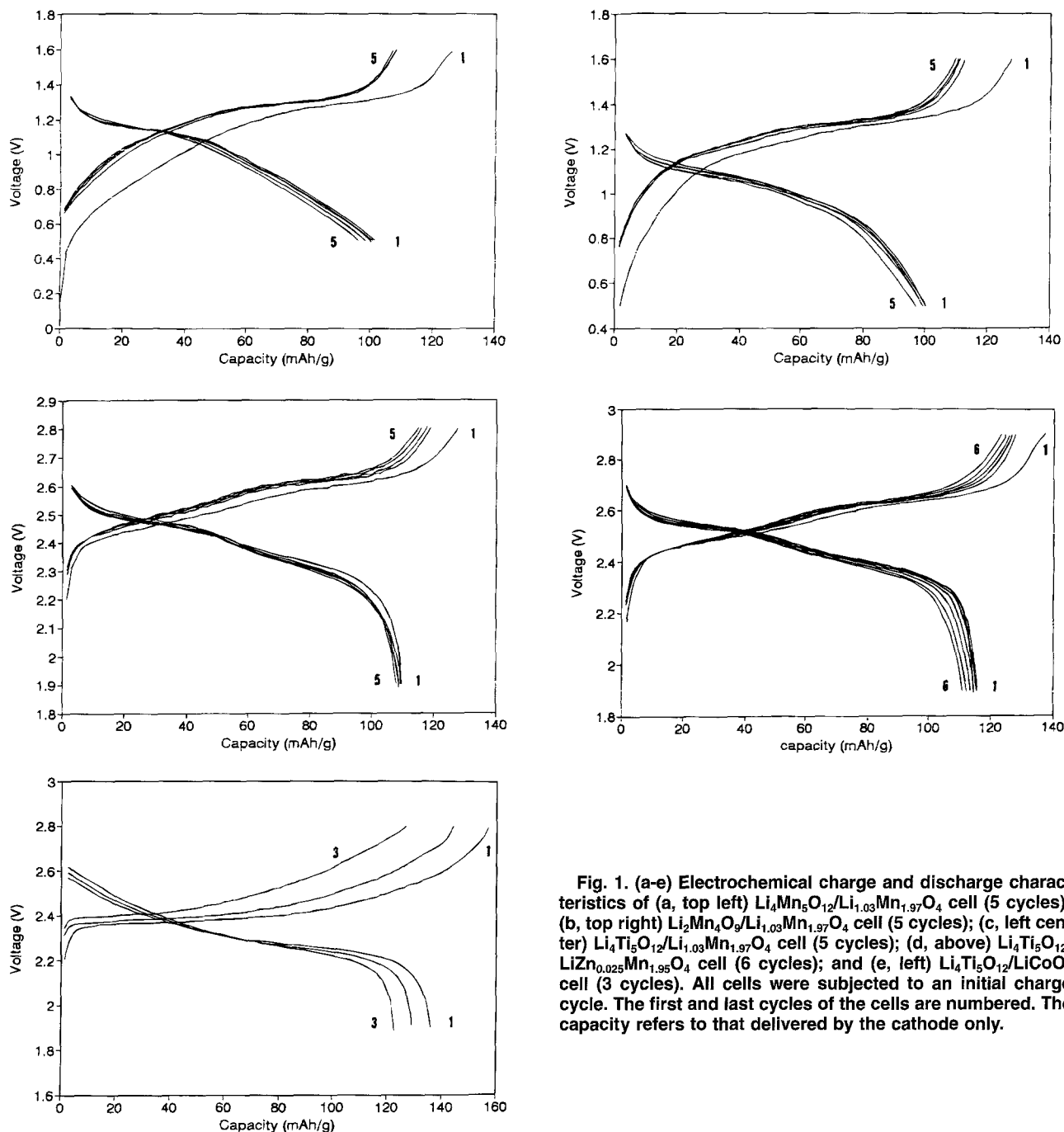
The electrochemical charge and discharge characteristics for the first five cycles of the Li<sub>4</sub>Mn<sub>5</sub>O<sub>12</sub>/Li<sub>1.03</sub>Mn<sub>1.97</sub>O<sub>4</sub> and Li<sub>2</sub>Mn<sub>4</sub>O<sub>9</sub>/Li<sub>1.03</sub>Mn<sub>1.97</sub>O<sub>4</sub> cells are shown in Fig. 1a, b. The cells were charged and discharged between upper and lower voltage limits of 1.6 and 0.5 V, respectively, at a current rate of 0.15 mA/cm<sup>2</sup>. In both cells, approximately 50% of the discharged capacity was delivered between 1.3 and 1.0 V; thereafter, the voltage dropped relatively quickly to 0.5 V. The total capacity delivered by each cell (100 mAh/g of cathode) reflects a 71% utilization of the cathode. Calculations based on reactions 1 and 2 and on an average operating voltage of 1 V indicate that balanced Li<sub>2</sub>Mn<sub>4</sub>O<sub>9</sub>/Li<sub>1.03</sub>Mn<sub>1.97</sub>O<sub>4</sub> and Li<sub>4</sub>Mn<sub>5</sub>O<sub>12</sub>/Li<sub>1.03</sub>Mn<sub>1.97</sub>O<sub>4</sub> cells will deliver an energy density of 49 and 48 Wh/kg, respectively, taking into consideration only the masses of the active electrode materials. The performance of these cells will, however, be limited by the instability of the organic electrolyte at low voltages, particularly below 0.5 V. From these data, it

Table III. Composition and theoretical capacity of anode and cathode materials.

Fully charged composition	Fully discharged composition	Theoretical capacity <sup>a</sup> (mAh/g)
<b>Anodes</b>		
Li <sub>7</sub> Mn <sub>5</sub> O <sub>12</sub>	Li <sub>4</sub> Mn <sub>5</sub> O <sub>12</sub>	156
Li <sub>5</sub> Mn <sub>4</sub> O <sub>9</sub>	Li <sub>2</sub> Mn <sub>4</sub> O <sub>9</sub>	202
Li <sub>7</sub> Ti <sub>5</sub> O <sub>12</sub>	Li <sub>4</sub> Ti <sub>5</sub> O <sub>12</sub>	168
<b>Cathodes</b>		
Li <sub>0.12</sub> Mn <sub>1.97</sub> O <sub>4</sub>	Li <sub>1.03</sub> Mn <sub>1.97</sub> O <sub>4</sub>	141
Li <sub>0.15</sub> Zn <sub>0.025</sub> Mn <sub>1.95</sub> O <sub>4</sub>	Li <sub>1.025</sub> Zn <sub>0.025</sub> Mn <sub>1.95</sub> O <sub>4</sub>	135
Li <sub>0.4</sub> CoO <sub>2</sub> <sup>b</sup>	LiCoO <sub>2</sub>	172

<sup>a</sup> Based on the mass of the fully charged composition.

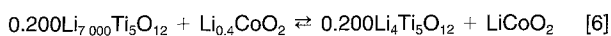
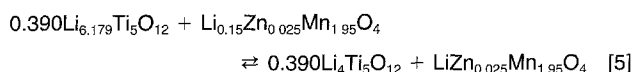
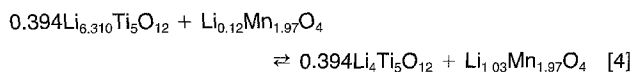
<sup>b</sup> The approximate composition of a fully delithiated and stable Li<sub>x</sub>CoO<sub>2</sub> compound.



**Fig. 1. (a-e) Electrochemical charge and discharge characteristics of (a, top left)  $\text{Li}_4\text{Mn}_5\text{O}_{12}/\text{Li}_{1.03}\text{Mn}_{1.97}\text{O}_4$  cell (5 cycles); (b, top right)  $\text{Li}_2\text{Mn}_4\text{O}_7/\text{Li}_{1.03}\text{Mn}_{1.97}\text{O}_4$  cell (5 cycles); (c, left center)  $\text{Li}_4\text{Ti}_5\text{O}_{12}/\text{Li}_{1.03}\text{Mn}_{1.97}\text{O}_4$  cell (5 cycles); (d, above)  $\text{Li}_4\text{Ti}_5\text{O}_{12}/\text{LiZn}_{0.025}\text{Mn}_{1.95}\text{O}_4$  cell (6 cycles); and (e, left)  $\text{Li}_4\text{Ti}_5\text{O}_{12}/\text{LiCoO}_2$  cell (3 cycles). All cells were subjected to an initial charge cycle. The first and last cycles of the cells are numbered. The capacity refers to that delivered by the cathode only.**

can be concluded, that these lithium cells will not compete with nickel-cadmium cells that operate at a similar voltage.

**2.5 V cells.**—The electrochemical charge and discharge curves for the first five or six cycles of the  $\text{Li}_4\text{Ti}_5\text{O}_{12}/\text{Li}_{1.03}\text{Mn}_{1.97}\text{O}_4$ ,  $\text{Li}_4\text{Ti}_5\text{O}_{12}/\text{LiZn}_{0.025}\text{Mn}_{1.95}\text{O}_4$ , and  $\text{Li}_4\text{Ti}_5\text{O}_{12}/\text{LiCoO}_2$  cells are given in Fig. 1c-e. The former two cells were charged and discharged at  $0.15 \text{ mA/cm}^2$ , whereas the current rate in the  $\text{Li}_4\text{Ti}_5\text{O}_{12}/\text{LiCoO}_2$  cell was  $0.1 \text{ mA/cm}^2$ . The upper voltage limit was set at either 2.8 or 2.9 V, and the lower limit at 1.9 V. The reactions for the three cells are



For reaction 4, the theoretical cell capacity and energy density (based on an average discharge voltage of 2.5 V) are 68 Ah/kg and 170 Wh/kg, respectively; for reaction 5 they are 63.5 Ah/kg and 159 Wh/kg, respectively. In reaction 6, the  $\text{Li}_4\text{Ti}_5\text{O}_{12}/\text{LiCoO}_2$  cell

operates at approximately 100 mV lower than the cells with manganese oxide cathodes. Nevertheless, because this cell has a higher theoretical capacity (85 Ah/kg) than the manganese oxide cells, it offers a higher energy density (203 Wh/kg), slightly higher than that of the nickel-cadmium cell (194 Wh/kg). Although these lithium cells lose capacity slowly on cycling, their performance can be expected to be enhanced with improved materials processing and cell design.

### Conclusions

Lithium-ion or rocking-chair cells with spinel anodes and transition-metal oxide cathodes have been fabricated and tested. Cells with  $\text{Li}_4\text{Ti}_5\text{O}_{12}$  anodes and spinel-related or  $\text{LiCoO}_2$  cathodes deliver energy densities comparable with a nickel-cadmium cell but at approximately twice the voltage. The fact that these cells produce no metallic lithium during charge makes them more attractive from a safety viewpoint compared to lithium cells that employ lithium or lithium-carbon anodes; they are, therefore, possible alternatives to nickel-cadmium cells.

### Acknowledgments

Manuscript submitted July 12, 1994; revised manuscript received Aug. 2, 1994.

Argonne National Laboratory assisted in meeting the publication costs of this article.

## REFERENCES

- M. M. Thackeray and J. B. Goodenough, U.S. Pat. 4,507,371 (1985).
- M. M. Thackeray, P. J. Johnson, L. A. de Picciotto, P. G. Bruce, and J. B. Goodenough, *Mater. Res. Bull.*, **19**, 179 (1984).
- M. M. Thackeray, W. I. F. David, P. G. Bruce, and J. B. Goodenough, *ibid.*, **18**, 461 (1983).
- T. Ohzuku, M. Kitagawa, and T. Hirai, *This Journal*, **137**, 769 (1990).
- J. M. Tarascon, E. Wang, F. K. Shokoohi, W. R. McKinnon, and S. Colson, *ibid.*, **138**, 2859 (1991).
- M. M. Thackeray, A. de Kock, M. H. Rossouw, D. C. Liles, D. Hoge, and R. Bittihn, *ibid.*, **139**, 363 (1992).
- R. J. Gummow, A. de Kock, and M. M. Thackeray, *Solid State Ionics*, **69**, 59 (1994).
- D. W. Murphy, R. J. Cava, S. M. Zahurak, and A. Santoro, *ibid.*, **9-10**, 413 (1983).
- K. M. Colbow, J. R. Dahn, and R. R. Haering, *J. Power Sources*, **26**, 397 (1989).
- L. A. de Picciotto and M. M. Thackeray, *Mater. Res. Bull.*, **20**, 1409 (1985).
- R. J. Gummow and M. M. Thackeray, *ibid.*, **27**, 307 (1992).
- R. J. Gummow and M. M. Thackeray, *Solid State Ionics*, **53-56**, 681 (1992).
- R. J. Gummow, D. C. Liles, M. M. Thackeray, and W. I. F. David, *Mater. Res. Bull.*, **28**, 1177 (1993).
- E. Rossen, J. N. Reimers, and J. R. Dahn, *Solid State Ionics*, **62**, 53 (1993).
- D. Fauteux and R. Koksang, *J. Appl. Electrochem.*, **23**, 1 (1993).
- S. Morzilli, B. Scrosati, and F. Sgarlatta, *Electrochim. Acta*, **30**, 1271 (1985).
- D. W. Murphy, F. J. Di Salvo, J. N. Carides, and W. V. Waszczak, *Mater. Res. Bull.*, **13**, 1395 (1978).
- T. Ohzuku, in Extended Abstracts of 7th International Meeting on Lithium Batteries, p. 111, Boston, May 15-20, 1994.
- A. de Kock, M. H. Rossouw, L. A. de Picciotto, M. M. Thackeray, W. I. F. David, and R. M. Ibberson, *Mater. Res. Bull.*, **25**, 657 (1990).
- JCPDS X-Ray Powder Diffraction File: 26-1198.
- JCPDS X-Ray Powder Diffraction File: 36-1004.
- R. J. Gummow, Ph.D. Thesis, University of Cape Town, Cape Town, South Africa (1993).

## Thermal Oxidation of SiC in N<sub>2</sub>O

R. C. De Meo,<sup>a</sup> T. K. Wang,<sup>a</sup> T. P. Chow,<sup>a</sup> D. M. Brown,<sup>b</sup> and L. G. Matus<sup>c</sup>

<sup>a</sup>Center for Integrated Electronics, Rensselaer Polytechnic Institute, Troy, New York 12180

<sup>b</sup>General Electric Corporation, Research and Development, Schenectady, New York 12301

<sup>c</sup>NASA Lewis Research Center, Cleveland, Ohio 44153

## ABSTRACT

Thermal oxidation kinetics of 3C and 6H-SiC in N<sub>2</sub>O at 1050 to 1150°C have been studied. The oxidation rate follows an unusual parabolic-linear relationship that has also been found for oxidation of silicon in N<sub>2</sub>O. The activation energy of the parabolic rate constant (*B*) is  $3.1 \pm 0.22$  eV/molecule for 3C-SiC, and  $4.80 \pm 1.02$  eV/molecule for 6H-SiC. The limiting mechanism for oxidation is attributed to the diffusion of CO through the oxynitride layer. 3C-SiC metal oxide semiconductor capacitors fabricated in N<sub>2</sub>O exhibit fixed oxide charge densities on the order of  $10^{12}$  cm<sup>-2</sup> and are slightly lower than those oxidized in steam.

There has been an increased effort to improve the characteristics of the SiC/SiO<sub>2</sub> interface for better device performance. Recent studies<sup>1</sup> have shown that thermal oxidation of Si in a N<sub>2</sub>O ambient has led to improved electrical characteristics of gate dielectrics in metal oxide semiconductor (MOS) devices. However, it has been shown that N<sub>2</sub>O oxidation of Si MOS structures have an increased fixed oxide charge density.<sup>2</sup> This Letter presents, for the first time, the oxidation kinetics and fixed oxide charge results of thermally grown N<sub>2</sub>O oxides on 3C-SiC. Results for 6H-SiC are presented for comparison.

### Experimental

Oxidation experiments were performed on 3C-SiC epitaxially grown by chemical vapor deposition (CVD) on (100) p-type Si substrates. The samples were tilted 1° off-axis. The 3C-SiC layer was ~2 μm thick and unintentionally doped n-type with a concentration ranging from  $10^{17}$  to  $10^{18}$  cm<sup>-3</sup>. The 6H-SiC samples were (100) Si face with  $N_d = 6 \times 10^{18}$  cm<sup>-3</sup>.

The samples were precleaned in the standard RCA sequence, followed by a dip in 20:1 HF to remove any native oxides. The samples were placed in a conventional resistive heating furnace at a standby temperature of 400°C. The furnace was elevated to the oxidation temperature at a rate of 10°C/min, with pure N<sub>2</sub> flowing at 50 lpm. After a stabilization step, oxidation was carried out in pure N<sub>2</sub>O (99%, U.S.P. grade). The furnace was then ramped down to 400°C at 5°C/min with pure N<sub>2</sub> flowing at 50 lpm. After oxidation, the film thickness and refractive index was measured by automated ellipsometry ( $\lambda = 632.8$  nm). The complex index of refraction of a bare 3C-SiC layer is  $2.6 - 0.05i$ .<sup>3</sup> It has been shown that no significant error is introduced when ellipsometry measurements are done on oxynitride samples without fixing the refractive index.<sup>4</sup> Cumulative oxidation runs were performed at 1050, 1100, and 1150°C to obtain oxide thicknesses up to 0.2 μm. Compositional depth profiling by secondary ion mass spectrometry (SIMS) was

performed on several samples to analyze the relative percentage of oxygen, carbon, and nitrogen.

MOS capacitors were also fabricated on 3C-SiC with gate oxides grown by four different methods: sample 1 was oxidized in wet O<sub>2</sub> at 1100°C; sample 2 was oxidized in an N<sub>2</sub>O ambient at 1150°C; sample 3 was first oxidized in N<sub>2</sub>O at 1150°C, and then an SiO<sub>2</sub> film of 22.0 nm was deposited by CVD; sample 4 was first oxidized in steam at 1150°C, and then reoxidized in N<sub>2</sub>O. Fixed oxide charge measurements were made using the dual-gate capacitor method.<sup>5</sup> The area of the small capacitor was  $3.14 \times 10^{-4}$  cm<sup>-2</sup>. The ratio of capacitor areas is 225:1.

### Results

The oxide thickness as a function of time for 3C-SiC, for the temperature range of 1050 to 1150°C, is shown in Fig. 1. The curves for 3C-SiC in N<sub>2</sub>O show an initial parabolic growth rate with a gradual shift to linear behavior for long oxidation times. This is consistent with the results for Si.<sup>6</sup> The different regimes are most pronounced at 1150°C and tend to disappear with decreasing temperature. Our results suggest oxidation of N<sub>2</sub>O may be due to two limiting mechanisms where one dominates for thin films and the other for thicker films. Since oxidation at 1050°C is neither linear or parabolic, it is reasonable to suspect that these reactions are temperature dependent. A thickness vs. time curve for 6H-SiC at 1150°C is also shown in Fig. 1. Large scatter in the data prevented us from obtaining consistent results for other 6H-SiC kinetic curves, 3C and 6H-SiC oxidation rates are much slower in N<sub>2</sub>O than in steam, oxygen, or N<sub>2</sub>O oxidation of Si.

The activation energy for the parabolic rate constants were extracted by regression analysis of the Arrhenius plot in Fig. 2. The activation energy is estimated to be  $3.1 \pm 0.22$  eV/molecule for 3C-SiC. This is higher than the 2.16 eV/molecule for the parabolic rate constant in wet oxidation of 3C-SiC.<sup>7</sup> It is suggested<sup>8</sup> that the limiting mechanism for the parabolic regime in wet oxidation is the